Optimizing Rice Husk Silica Mass and Sonication Time for a More Efficient and Environmentally Friendly Synthesis of SBA-15

Suyanta Suyanta* and Mudasir Mudasir

Department of Chemistry, Faculty of Mathematics and Natural Sciences, Universitas Gadjah Mada, Sekip Utara, Yogyakarta 55281, Indonesia

* ***Corresponding author:***

email: suyanta_mipa@ugm.ac.id

Received: February 25, 2022
Accepted: May 4, 2022

DOI: 10.22146/ijc.73258

Abstract: *By optimizing rice husk silica mass and sonication time, SBA-15 was successfully synthesized in a more efficient and environmentally friendly way. The solution of Pluronic P-123 was mixed with the solution containing NaOH and various masses of rice husk silica (4–12 g), followed by sonication for a certain time (30–150 min). The mixture was filtered and washed with distilled water and ethanol until neutral, then dried at 110 °C for 2 h and calcined at 500 °C for 6 h. The results showed that the optimal mass of rice husk silica was 8 g, while the optimal sonication time was 30 min. The product has a cylindrical pore shape with good crystallinity and pore structure regularity. The specific surface area (S_{BET}), the pore diameter (D_{BJH}), the specific pore volume (V_{BJH}), and the wall thickness (W_T) of the product were 601 $m^2\ g^{-1}$, 4.76 nm, 0.88 mL g^{-1}, and 5.02 nm, respectively. These results are not considerably different from the porosity of SBA-15, synthesized previously using conventional hydrothermal techniques from various silica sources. In addition, it is also comparable to the porosity of SBA-15 produced from TEOS by sonochemical methods as well as with commercial SBA-15.*

Keywords: *rice husk silica; SBA-15; optimization; mass; sonication time*

■ INTRODUCTION

The mesoporous silicate family, which includes Santa Barbara Amorphous No. 15 (SBA-15), folded sheet mesoporous material No. 16 (FSM-16), and the M4IS family (Mobil Composition of Matter No. 41, MCM-41; Mobil Composition of Matter No. 48, MCM-48; and Mobil Composition of Matter No. 50, MCM-50) has attracted the attention of researchers to the point where it now occupies a superposition in materials science because of its potential to be applied in various fields. As a material having a regular pore structure with a diameter of 2–50 nm, it can minimize crystal formation, inhibit nanoparticle aggregation, stabilize the position, and improve the special surface of the material. Therefore, it can be used in various surface-related applications, such as catalysis [1-3], gas separation [4-7], drug delivery [8-9], energy storage [10-11], membranes [12-13], and sensors [14-15]. According to their pore size, mesoporous silicates can provide access to relatively large molecules and enhance diffusion. This is an advantage when compared to micro materials such as zeolites [16]. SBA-15 was originally synthesized by Zhao et al. [17] using a poly(ethylene oxide)-poly(propylene oxide)-poly(ethylene oxide) template commercially known as Pluronic P-123. SBA-15 has a two-dimensional hexagonal pore shape similar to MCM-41, but it has tiny mesopores on the pore walls that link parallel mesopores [18-19]. As a result, SBA-15 outperforms MCM-41 in terms of adsorbent and catalyst applications. Furthermore, the SBA-15 family has thicker pore walls, resulting in superior thermal and hydrothermal stability than the M41S and FSM-16 families [20-22].

In general, commercial materials such as tetraethyl orthosilicate (TEOS) [23-25] and sodium silicate [26-27] are utilized as silica precursors in the production of SBA-15, which are, of course, relatively expensive. Several natural materials have been used as a source of silica in the synthesis of SBA-15, including sugarcane bagasse [28], brickyard ash [29], coal gangue [30], oil palm ash [31], and rice husk ash [32-34], to reduce production

costs. Rice husk ash is the most potent natural material because it contains more than 90% of SiO_2 [35-37]. Moreover, rice is widely grown in Asian countries such as China, India, Pakistan, Cambodia, Indonesia, Laos, Malaysia, Myanmar, Philippines, Thailand, Vietnam, etc. [38], giving large opportunity to use the rice husk ash as the source of silica in the synthesis of SBA-15. According to Barrera et al. [39], the silica/surfactant ratio has a significant impact on the mechanism of mesoporous development in the synthesis of SBA-15. Other report suggests that a low silica/surfactant ratio causes the mesoporous material to be difficult to create, but a high ratio causes the structure's regularity to be compromised [40]. Therefore, it is quite clear that the silica/surfactant ratio is one of the important key factors in the successful synthesis of SBA-15. However, to the best of our knowledge, the report that deals with the optimization of the silica/surfactant ratio, especially in cases where rice husk silica is used as the source of silica, is rarely found. Therefore, in order to obtain the best ratio of silica/surfactant in the more efficient synthesis of SBA-15 from rice hush ash, it is quite challenging to conduct research on the optimization of the silica/surfactant ratio.

SBA-15 is typically synthesized using the hydrothermal technique [23-34], which involves heating the reactants with air in a closed container (autoclave). The hydrothermal approach is less cost-effective and does not adhere to the green chemistry principle since it takes a long time and a lot of energy to complete the reaction. Several studies have used alternative methods to synthesize SBA-15, such as the sonochemical approach, which involves the use of ultrasonic waves [41-45]. Ultrasonic waves can cause chemical reactions in liquids by causing micro-cavitation bubbles to develop. High temperatures and pressures can be produced by burst bubbles, allowing chemical reactions to take place [46]. Because it consumes less time and energy, the sonochemical approach is considered as more cost-effective and supports green chemistry principles.

The sonication time affects product quality in the synthesis of several materials; for example, the thermal stability of the product in the synthesis of polystyrene/montmorillonite nanocomposites [47], the morphology and dispersion of the product in the synthesis of cellulose nanocrystals [48], the specific surface area of the product in the synthesis of micron-sized vermiculite particles [49], the properties of the product in the synthesis of methylcellulose-montmorillonite films [50], and so on. In case of SBA-15 synthesis, Chaeronpanich et al. [51] has reported that increasing sonication time could increase the specific surface area, specific pore volume, and pore diameter of the product. Unfortunately, there is still no report that focuses on the optimization of sonication time in the synthesis of SBA-15 using rice husk silica as a precursor. The information about the effect of sonication time on the efficiency of the SBA-15 synthesis is essential to reduce the time and energy required for the synthesis.

Therefore, based on the above-mentioned ideas, we report the results of our systematic study on the optimization of the rice husk silica to surfactant ratio (Pluronic P-123) as well as the optimization of the sonication time to obtain a more efficient and environmentally friendly SBA-15 synthesis method. Optimization of the ratio of rice husk silica to Pluronic P-123 was carried out by varying the mass of rice husk silica for a certain number of Pluronic P-123 surfactants. The characterization data of SBA-15 synthesized in this study were compared to SBA-15 synthesized previously using conventional hydrothermal techniques from various silica sources. More specifically, the data was also compared with SBA-15 produced from TEOS by sonochemical methods as well as with commercial SBA-15.

■ EXPERIMENTAL SECTION

Materials

The rice husk was taken from the rice huller in the districts of Klaten, Central Java, Indonesia. Chemicals used in this study were purchased from Merck (Germany), i.e., Pluronic P-123 (M-Clarity™ quality level = MQ100, MW: 5800 g/mol), HCl (37%), NaOH (100%), toluene (99.5%), ethanol (96%). All of the chemicals are analytical reagent grade and used without further purification. Distilled water was used in all experiments.

Instrumentation

Ultrasonic emission is performed using a Bransonic 220 ultrasonic instrument (Taiwan) with a frequency of 48 kHz and a heating power of 100 W at a room temperature (25 to 32 °C). X-ray diffraction (XRD) patterns were recorded at room temperature using Cu K powder irradiated at = 0.154 nm on an X-ray diffractometer, Shimadzu 6000 (Japan). A Shimadzu FTIR Prestige-21 (Japan) was used to measure a Fourier-transform infrared (FTIR) spectroscopic spectra, which were acquired in the transmittance mode in the range of 4000–400 cm^{-1} at room temperature using the KBr disc pellets. The nitrogen adsorption-desorption isotherm was measured at liquid nitrogen temperature using a Quantachrome NovaWin2 version 2.2 (USA). Samples were outgassed overnight at 250 °C before measurement. Using adsorption data at a relative pressure (P/P_0) of 0.03 to 0.1, the Brunauer–Emmett–Teller (BET) surface area is calculated using the multipoint BET method. At a relative pressure of 0.95, isotherms were used to calculate a mesoporous volume. The Barrett-Joyner-Halenda (BJH) approach was used to calculate the average mesoporous diameter based on the nitrogen isotherm adsorption branch. The pore size distributions were calculated using the BJH model. Transmission electron microscopy (TEM) JEOL JEM-1400 (USA) was used to examine the features of the SBA-15 pores.

Procedure

Extraction of silica from rice husk

Rice husk (2 kg) was washed with water, dried in the sun, and then burned to ashes in the open air. This ash (100 g) is placed in 125 mL of concentrated HCl which has been diluted to 500 mL with distilled water. To make rice husk silica, the mixture was agitated at 60 °C for 3 h, then filtered with Whatman 42 filter paper, rinsed with distilled water, dried at 120 °C for 24 h, then calcined at 600 °C for 6 h. FTIR and XRD were used to characterize the product.

Synthesis of SBA-15 with variations in the mass of rice husk silica

To make a sodium silicate solution, 4 g of rice husk silica, and 10 g of NaOH were added to the distilled water (100 mL). The mixture was agitated for 2 h at 80 °C, and then incubated for 12 h. Pluronic P-123 (4 g) was dissolved in 100 mL of 1.6 M HCl, then heated to 45 °C while stirring to dissolve it. The sodium silicate solution (100 mL) was added to the Pluronic P-123 solution (100 mL), then was sonicated for 60 min and heated at 60 °C for 1 h. After filtering the mixture with Whatman 42 filter paper, it was rinsed with distilled water and ethanol until the pH was neutral. The resulting solid was dried at 110 °C for 2 h, then calcined at 500 °C for 6 h to produce a white powder denoted as SBA-15 (4 g, 60 min). The same procedure was done 4 times with different amounts of rice husk silica (6, 8, 10, and 12 g, respectively). The resulting material was denoted as SBA-15 (6 g, 60 min), SBA-15 (8 g, 60 min), SBA-15 (10 g, 60 min), and SBA-15(12 g, 60 min), respectively. The methods of FTIR, XRD, GSA, and TEM were used for characterization of the product.

Synthesis of SBA-15 with variations in sonication time

The procedure of SBA-15 synthesis above was carried out four times, each time with the optimal mass of rice husk silica and a sonication time of 30, 90, 120, and 150 min, respectively. The materials were labeled as SBA-15 (X g, 30 min), SBA-15 (X g, 90 min), SBA-15 (X g, 120 min), and SBA-15 (X g, 150 min), respectively, where X represents the optimal mass of rice husk silica.

■ RESULTS AND DISCUSSION

Rice Husk Silica

The silica extracted from rice husk is in the form of a white powder, which matches nicely the properties and color of commercial silica [52]. The FTIR spectra of rice husk silica and commercial silica (for comparison) are presented in Fig. 1. It is easily seen that the two spectra are closely resemble one each other, indicating the success of silica extraction from rice husk. Table 1 gives some distinctive bands for siloxane groups (Si–O–Si) and silanol groups (Si–OH) in the rice husk silica.

The XRD patterns for both rice husk silica and commercial silica (Fig. 2) reveal broad peaks around 23°, which are typical of amorphous silica [52], suggesting that the extraction of silica from rice husks has been

successfully carried out. This XRD pattern data supports the FTIR spectra, suggesting the success of silica extraction form rice husk.

SBA-15 Synthesized by Varying the Volume of Sodium Silicate

FTIR spectra analysis

The FTIR spectra of SBA-15 produced with varying amounts of sodium silicate and those of commercial SBA-15 are given in Fig. 3. Both spectra show multiple characteristic absorption bands for mesoporous silicates dominated by siloxane (Si–O–Si) and silanol (Si–OH) groups, similar to the spectra of rice husk silica. Furthermore, due to Si–O stretching vibration on the silanol group, absorption exhibits around 970 cm^{-1} [55]. The broad peak at 3460 cm^{-1} belongs to the remaining absorbed water molecules in the samples overlapped with the O–H bond stretching vibration of the silanol groups [56]. The bending vibration of the O–H of water appears at wavenumber 1635 cm^{-1} [54,57]. The strong characteristic peak of siloxane (Si–O–Si) appears at 1082 cm^{-1} [53]. The rocking vibration of the Si–O bond is observed at 490 cm^{-1} [53]. On the basis of these data, it can be stated that the use of sodium silicate solution with a mass of 4, 6, 8, 10 and 12 g in this study has resulted in a material containing a –Si–O–Si– network and a Si–OH group.

The spectra of SBA-15 (4 g, 60 min) and SBA-15 (12 g, 60 min) show a lower absorption intensity, indicating that the formation of the –Si–O–Si– network and the Si–OH group in the two samples is not flawless. This is most likely caused by a very low or very high-mass ratio of silica to surfactant in these two samples. The formation of the –Si–O–Si– network and the –Si–OH group can be hampered by a silica/surfactant ratio that is either too small or too large [39]. On the other hand, the samples of SBA-15 (6 g, 60 min), SBA-15 (8 g, 60 min), and SBA-15 (10 g, 60 min) exhibit relatively high absorption intensities, indicating that the –Si–O–Si– network and

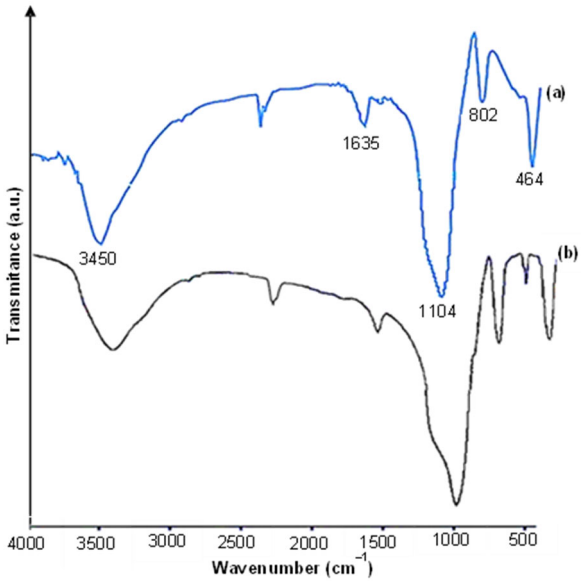

Fig 1. FTIR spectra of rice husk silica (a) and commercial silica (b)

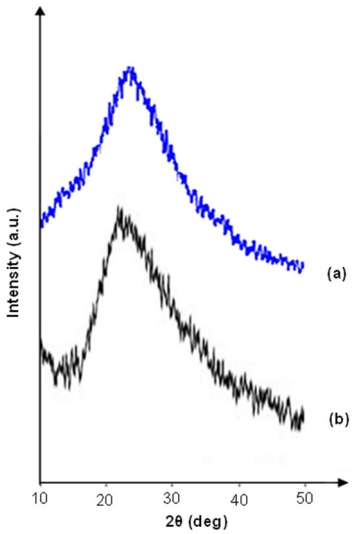

Fig 2. XRD diffractograms of rice husk silica (a) and commercial silica (b)

Table 1. Important FTIR absorption bands of rice husk silica and their interpretation

No	Wavenumber	Interpretation	Reference
1	464 cm^{-1}	Rocking vibration of Si–O bond	[53]
2	802 cm^{-1}	Symmetric stretching vibration of Si–O–Si	[53]
3	1104 cm^{-1}	Asymmetric stretching vibration of Si–O–Si	[53]
4	1635 cm^{-1}	Bending vibration of the O–H of water	[54]
5	3448 cm^{-1}	O–H Vibrations of silanol groups and adsorbed water	[54]

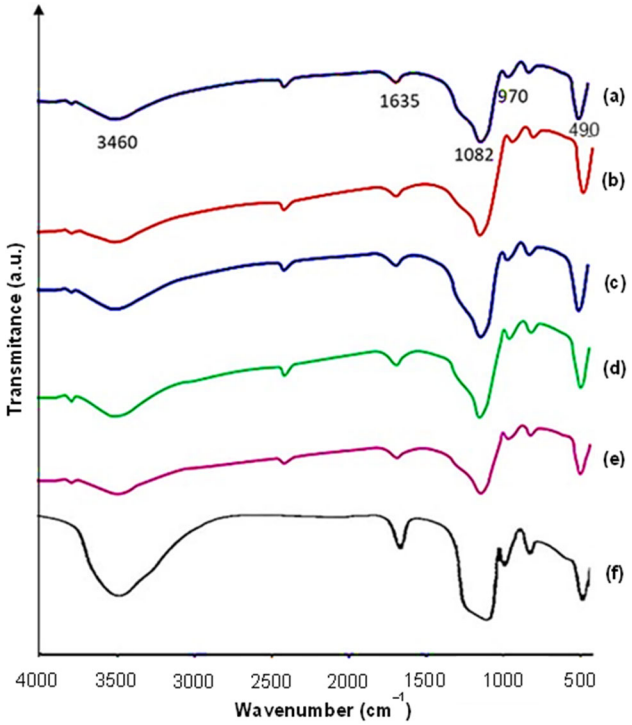

Fig 3. The FTIR spectra of: (a) SBA-15 (4 g, 60 min), (b) SBA-15 (6 g, 60 min), (c) SBA-15 (8 g, 60 min), (d) SBA-15 (10 g, 60 min), and (e) SBA-15 (12 g, 60 min), and (f) commercial SBA-15

–Si–OH are well-formed. Because FTIR spectra only provide information on the functional groups present in a material, FTIR alone is insufficient to draw a conclusion about the appropriate mass of rice husk silica in the synthesis of SBA-15. Therefore, more diverse characterization data generated by other analytical methods are necessary.

XRD pattern analysis

Fig. 4 shows the effect of rice husk silica mass used in the synthesis on the number, diffraction angle, and intensity of diffractogram peaks. The diffractogram of commercial SBA-15 is also presented as a reference. The peaks of [100] are found in all of the diffractograms, which are typical of 2D hexagonal formations. The peak number for diffractogram of SBA-15 (4 g, 60 min) is limited to only one peak, [100] with quite low intensity. This is probably due to insufficient amount of silica present in the sample, preventing the creation of micelles that serve as the hexagonal structural template [39]. On the other hand, each diffractogram of SBA-15 (6 g, 60 min), SBA-15 (8 g, 60 min), SBA-15 (10 g, 60 min), and commercial SBA-15 contains three peaks ([100], [110], and [200]), whereas the SBA-15 (12 g, 60 min) diffractogram exhibits two peaks ([100] and [110]). The presence of additional peaks in the diffractograms, especially peaks [110] and [200], suggests the occurrence of mesoporous regularity growth in the samples [39].

The diffraction angle of [100] peak gets bigger in the order of SBA-15 (4 g, 60 min) < SBA-15 (6 g, 60 min) < SBA-15 (8 g, 60 min) < SBA-15 (10 g, 60 min), but gets smaller at SBA-15 (12 g, 60 min). The diffraction angle is inversely proportional to the interplanar spacing (d_{100}), where the d_{100} decreases as the diffraction angle increases. So, it can be concluded that the use of more rice husk silica, from 4 to 10 g, d_{100} gives rise to a smaller d-spacing, but the use 12 g results in a bigger d-spacing. The similar trends have also been reported by Mendelez-Ortiz et al. [57]. The value of d_{100} can be used to obtain the lattice parameters a_o (where $a_o = 2d_{100}/\sqrt{3}$), which can

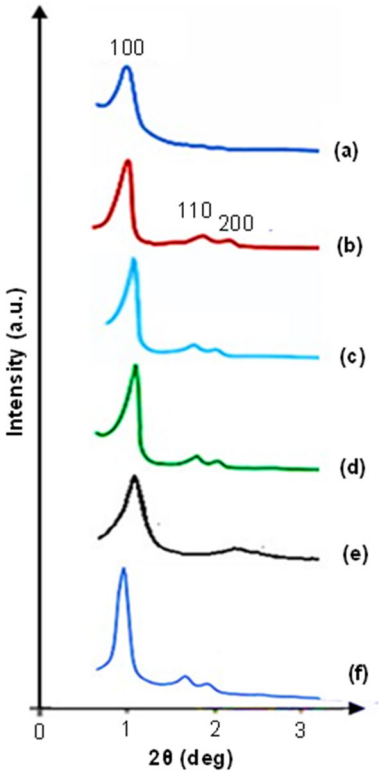

Fig 4. The XRD diffractogram of: (a) SBA-15 (4 g, 60 min), (b) SBA-15 (6 g, 60 min), (c) SBA-15 (8 g , 60 min), (d) SBA-15 (10 g, 60 min), and (e) SBA-15 (12 g, 60 min), and (f) commercial SBA-15

then be used to calculate the pore wall thickness (W_T) using the equation $W_T = a_0 - D_{BJH}$, where D_{BJH} is the average pore diameter acquired from the GSA data.

The peak intensity, especially the main peak [100] indicates the crystallinity of SBA-15 [58]. Fig. 4 demonstrates that the crystallinity of each sample produced in this study is still lower than that of commercial SBA-15. For the synthesized samples, the peak intensity [100] rose as the mass of rice husk silica used increased (from 4, 6, 8, and 10 g), but reduced when 12 g was used. This shows that the crystallinity of SBA-15 grew as the mass of rice husk silica used increased but declined as the mass of rice husk silica used climbed too high. A similar thing has been documented by other studies [39]. Based on the discussion on the FTIR spectra and XRD diffractogram, it can be stated that SBA-15 materials which have high crystallinity and relatively good hexagonal structure regularity are SBA-15 (6 g, 60 min), SBA-15 (8 g, 60 min), and SBA-15 (10 g, 60 min). These three samples were further analyzed quantitatively using a GSA to determine their porosity.

Gas adsorption analysis

The adsorption-desorption isotherms of the SBA-15 (6 g, 60 min), SBA-15 (8 g, 60 min), and SBA-15 (10 g, 60 min) samples are shown in Fig. 5 together with the isotherm of commercial SBA-15 for the purpose of comparison. According to the IUPAC classification, all four curves are classified as type IV, which is typical of mesoporous materials [59-60]. Generally, these isotherms exhibit a similar trend, which has five stages. There is a considerable increase in the volume of N_2 adsorbed at a relative pressure of 0.03 to 0.1, indicating the presence of single-layer N_2 adsorption on the surface of SBA-15, including external and internal surfaces. This stage is used as the basis for measuring the pore surface area using the BET method. Furthermore, the adsorption curve rises at a relative pressure of roughly 0.4, indicating the presence of multilayer N_2 adsorption across the entire surface. Because of the condensation of N_2 in the capillaries included in SBA-15, the adsorption curve dramatically increased at a relative pressure of about 0.4–0.7. The curve is nearly gentle at relative pressures above 0.6, indicating that only a little quantity of N_2 is adsorbed. Only the exterior

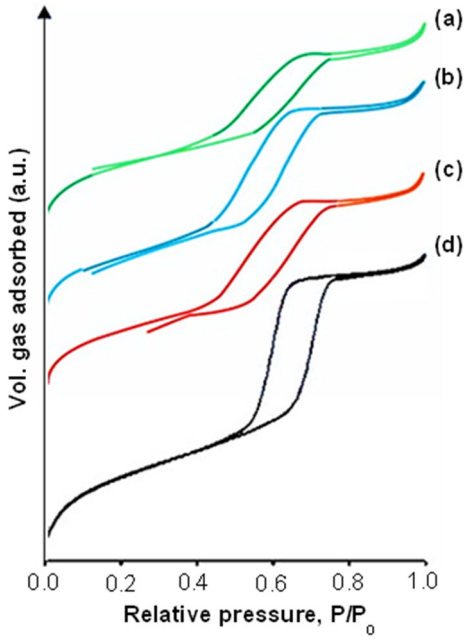

Fig 5. The adsorption-desorption isotherms of: (a) SBA-15 (6 g, 60 min), (b) SBA-15 (8 g, 60 min), (c) SBA-15 (10 g, 60 min), and (d) commercial SBA-15

surface of SBA-15 can still adsorb nitrogen molecules at this point. The short slope of the curve at this point illustrates the limited exterior surface area of the materials. Finally, due to the adsorption of N_2 in the interparticle region, the re-adsorption curve increases slightly for relative pressures close to 1.

A formation of hysteresis loop when the pressure is reduced, suggesting that the volume of desorbed gas does not equal the volume of adsorbed gas. This can happen as a result of the previously described capillary condensation. The hysteresis loop in the three samples of SBA-15 in this study is type H1 which is characteristic of mesoporous materials with one-dimensional cylindrical channels open on both sides [61]. For all the samples, type IV isotherms with steep H1 hysteresis loops at relative pressure P/P_0 of 0.4–0.8 can be observed, implying the formation of a uniform large mesopore. The bigger the pore diameter, the further right the inflection location, whereas the sharpness of the curve after the inflection reflects the uniformity of the mesoporous size distribution [62]. Furthermore, at this stage, the height of the curve is proportional to the pore volume of the materials. From Fig. 5, it is observed that

the distribution of mesoporous size is relatively uniform but the uniformity is slightly lower compared to commercial SBA-15.

The porosity of the SBA-15 (6 g, 60 min), SBA-15 (8 g, 60 min), and SBA-15 (10 g, 60 min) samples are shown in Table 2 together with the porosity of commercial SBA-15 for the purpose of comparison. The porosity data of the four samples (Table 2) reveal that the S_{BET} and V_{BJH} trends follow the crystallinity trend, according to the order Commercial SBA-15 > SBA-15 (8 g, 60 min) > SBA-15 (10 g, 60 min) > SBA-15 (6 g, 60 min). The crystallinity trend, however, does not appear to be related to both of the D_{BJH} as well as the W_T trend.

Fig. 6 shows that the commercial SBA-15 has a narrow pore size distribution with the highest intensity of about 5 nm, while the samples SBA-15 (6 g, 60 min), SBA-15 (8 g, 60 min), and SBA-15 (10 g, 60 min) had relatively wide pore size distributions with the highest intensity of about 4.3, 4.1, and 3.5 nm, respectively. This is supported by the XRD diffractogram in Fig. 4, which shows that the commercial SBA-15 diffractogram contains three peaks with the highest intensity when compared to other samples. Among the three samples synthesized with variations in the mass of rice husk silica, SBA-15 (10 g, 60 min) was the most homogeneous sample, characterized by a narrower curve with higher peaks. As for the samples of SBA-15 (6 g, 60 min) and SBA-15 (8 g, 60 min), the pore size distribution was more varied, with short and wide peaks. The pore diameter with the highest intensity on each curve is slightly different when compared to the average pore diameter of each sample in Table 2. This is because the average pore diameter covers all the pores in each sample.

Based on the porosity data in Table 2 and the pore size distribution in Fig. 6, it is evident that each synthesized sample has its own advantages in certain parameters, and no sample excels in all parameters. Although the SBA-15 (6 g, 60 min) sample has the biggest pore diameter and thickest pore wall, it has the smallest specific surface area and specific pore volume. Although the SBA-15 (6 g, 60 min) sample has the biggest

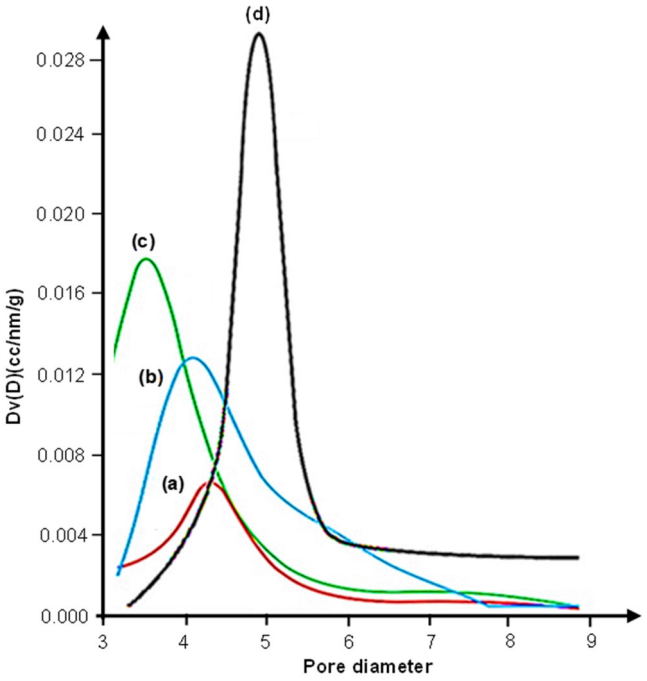

Fig 6. Pore size distribution of (a) SBA-15 (6 g, 60 min), (b) SBA-15 (8 g, 60 min), (c) SBA-15 (10 g, 60 min), and (d) Commercial SBA-15 samples

Table 2. The porosity of SBA-15 (6 g, 60 min), SBA-15 (8 g, 60 min), SBA-15 (10 g, 60 min), and commercial SBA-15

Sample	S_{BET} (m^2/g)	D_{BJH} (nm)	V_{BJH} (mL/g)	d_{100} (nm)	a_0 (nm)	W_T (nm)
SBA-15 (6 g, 60 min)	325	4.79	0.37	9.58	11.66	6.87
SBA-15 (8 g, 60 min)	652	3.98	0.65	8.89	10.27	6.29
SBA-15 (10 g, 60 min)	626	3.52	0.56	8.27	9.55	6.03
Commercial SBA-15	660	6.21	0.98	10.63	12.28	6.07

S_{BET} : specific surface area, BET
D_{BJH} : pore diameter, BJH adsorption
V_{BJH} : specific pore volume
d_{100} : interplanar spacing
a_o : lattice parameter, for hexagonal = $2d_{100}/\sqrt{3}$
W_T : silica wall thickness, for hexagonal $W_T = a_0 - D_{BJH}$

specific surface area and specific pore volume, the pore diameter is smaller and the pore walls are thinner than the SBA-15 (6 g, 60 min) sample. Moreover, although the SBA-15 (10 g, 60 min) sample has a narrower pore size distribution, it has flaws in several other characteristics. Nevertheless, the SBA-15 (8 g, 60 min) sample has been chosen as the one out of the three with the best accumulative porosity properties. The reasons for this choice are that the sample has the largest specific surface area and specific pore volume, while the pore diameter and pore wall thickness were not significantly different from that of the SBA-15 (6 g, 60 min) sample. In addition, the pore size distribution was better than that of the SBA-15 (6 g, 60 min) sample although it is not as good as that of the SBA-15 (10 g, 60 min) sample. For further experiments, we have only focused on the study of the effect of sonication time on the effectiveness of the synthesis of SBA-15 using an 8 g rice husk silica.

Effect of Sonication Time on the Synthesis Efficiency of SBA-15

FTIR spectra analysis

The FTIR spectra of SBA-15 produced with varying sonication times and those of commercial SBA-15 were presented in Fig. 7. This figure revealed distinctive absorptions for the siloxane and silanol groups, which were nearly identical to those shown in Table 1. The high intensity of these absorptions indicated the successful formation of –Si–O–Si– and Si–OH groups in all variations of sonication time. The spectra of the six FTIR appeared to be identical to one another, with no new absorption band shifts or substantial wavenumber shifts. The difference may be seen in the intensity of the absorption band, particularly at wavenumbers around 1096 cm^{-1}. The intensity of the absorption band decreased little as the sonication time increased from 30 to 150 min. So it can be stated that the sonication time of 30 min resulted in the formation of the most perfect –Si–O–Si– network, whereas extending the sonication time resulted in damage to portions of the –Si–O–Si– network.

Fig. 8 show the effect of sonication time on the number, diffraction angle, and intensity of the diffractogram peaks. The diffractogram of commercial

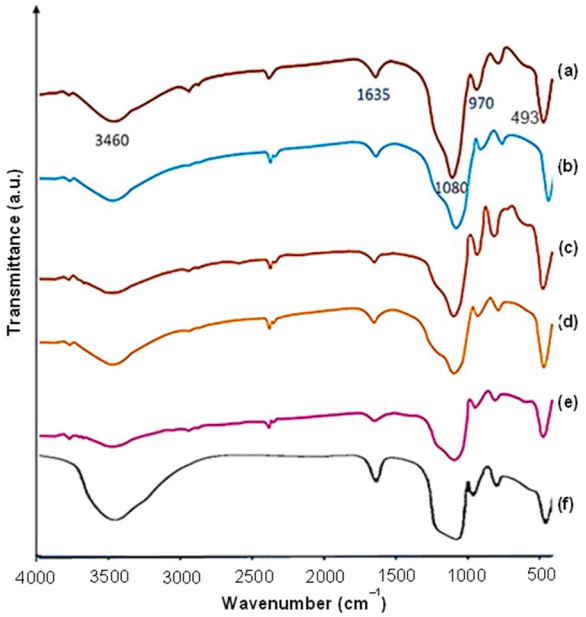

Fig 7. The FTIR spectra of: (a) SBA-15 (8 g, 30 min), (b) SBA-15 (8 g, 60 min), (c) SBA-15 (8 g, 90 min), (d) SBA-15 (8 g, 120 min), (e) SBA-15 (8 g, 150 min), and (f) commercial SBA-15

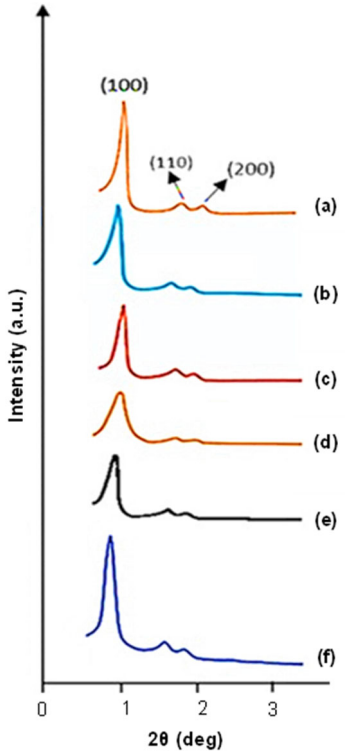

Fig 8. The XRD diffractogram of: (a) SBA-15 (8 g, 30 min), (b) SBA-15 (8 g, 60 min), (c) SBA-15 (8 g, 90 min), (d) SBA-15 (8 g, 120 min), and (e) SBA-15 (8 g, 150 min)

SBA-15 is also presented as a reference. The existence of three diffractogram peaks, [100], [110], and [200], was seen in all diffractograms, showing that the mesoporous silicate SBA-15 could be produced with any sonication time utilized in this investigation.

The 2θ of these diffractograms are 1.04, 0.99, 1.020, 0.97, and 0.96 for the sonication time of 30, 60, 90, 120, and 150 min, respectively. It is clear that except for the increase in sonication time from 60 to 90 min, where the peak changed to the right, the diffractogram's peak location shifted to the left as the sonication time was increased. The d_{100} samples can be obtained quantitatively using Bragg's Equation [63]: $\lambda = 2d_{100}\sin\theta$, where λ = wavelength of X-ray (0.154 nm), and θ = diffraction angle. So, we find the d_{100} are 8.47, 8.89, 8.62, 9.06, and 9.18 nm for sonication times of 30, 60, 90, 120, and 150 min, respectively. In general, increasing the sonication time increases the d_{100}, except for increasing the sonication time from 60 to 90 min. Mendelez-Ortiz et al. [57] reported similar results, where the value of d_{100} generally increased with increasing reaction time.

Fig. 8 indicates a drop in peak intensity [100] as sonication time is increased from 30 to 60, 90, and 120 min, but an increase when sonication time is raised to 150 min. This indicates that the crystallinity of SBA-15 varies, as evidenced by fluctuations in the [100] peak intensity. The highest peak intensity was produced if the sonication time was decreased to 30 min, which was getting closer to the intensity of commercial SBA-15. Table 3 shows the results quantitatively compared to commercial SBA-15, wherewith the sonication times of 30, 60, 90, 120, and 150 min, the relative crystallinities were 87.51, 74.81, 60.63, 35.64, and 43.26%, respectively. It was mean that with increasing sonication time, there is a trend of decrease in relative crystallinity. This is in line with the findings of On et al. [64], who found that a long sonication period might produce hydrolysis, which damages the pore wall and reduces pore size.

The higher energy received by the SBA-15 material, which is created together with the longer sonication time, can also cause damage to the pore structure. However, it appears that silicate anions formed by hydrolysis and exposed to sonication energy can polymerize again to form siloxane groups, resulting in a considerable increase in crystallinity when 150 min of sonication time. Perhaps, there is competition between the hydrolysis and deconstruction of siloxane groups by energy exposure on the one hand, with the polymerization process of silicate anions forming new siloxane groups on the other. Several earlier studies [65-67] also found that increasing sonication time or hydrothermal duration increased or decreased product crystallinity in the synthesis of various materials.

According to the FTIR spectra and XRD diffractogram analysis, the samples of SBA-15 (8 g, 30 min), SBA-15 (8 g, 60 min), and SBA-15 (8 g, 90 min) show outstanding crystallinity and usually high hexagonal structure regularity. These three samples were quantitatively evaluated using a gas sorption analyzer to determine the porosity.

Gas adsorption analysis

The adsorption-desorption isotherms of the SBA-15 (8 g, 30 min), SBA-15 (8 g, 60 min), and SBA-15 (8 g, 90 min) samples are shown in Fig. 9 together with the isotherm of commercial SBA-15 for the purpose of comparison. The curves of all samples exhibit a type IV isotherm which is characteristic for mesoporous materials. In general, the isotherm curves in this figure are not different to the type IV curve of Fig. 5. However, Fig. 9(a) reveals a distinct difference, in which the inflection point shifts to the right, and both the slope and height of the curve increase. It is indicating that the material has a larger pore diameter, more uniform mesopore, and a higher pore volume. In addition, the

Table 3. The relative crystallinity of SBA-15 synthesized with variation of sonication time compared to commercial SBA-15

Sample	Intensity (counts)	Relative crystallinity (%)*
Commercial SBA-15	2009	100
SBA-15 (8 g, 30 min)	1758	87.51
SBA-15 (8 g, 60 min)	1503	74.81
SBA-15 (8 g, 90 min)	1218	60.63
SBA-15 (8 g, 120 min)	716	35.64
SBA-15 (8 g, 150 min)	869	43.26

* compared to commercial SBA-15

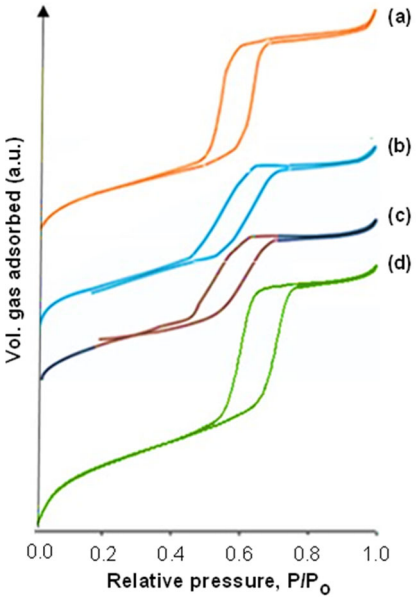

Fig 9. The adsorption-desorption isotherm of (a) SBA-15 (8 g, 30 min), (b) SBA-15 (8 g, 60 min), (c) SBA-15 (8 g, 90 min), and (d) commercial SBA-15

appearance of curve 9(a) more closely resembles the isothermal curve of commercial SBA-15 (Fig. 9(d)). This indicated that the sample has a diameter, volume, and uniformity of pores that are closer to the commercial SBA-15 as shown in Table 4 and Fig. 11.

The porosity of the four materials (Table 4) shows that the order of the specific surface area (S_{BET}) from large to small is Commercial SBA-15 > SBA-15 (8 g, 90 min) > SBA-15 (8 g, 60 min) > SBA-15 (8 g, 30 min). It is clear that the SBA-15 materials increase in specific surface area with increasing sonication time. A similar case was also reported by Chaeronpanich [51]. However, the difference in specific surface area in the present study is not significant, and each has a fairly large surface area (> 600 m^2/g). The order of pore diameters from large to small is Commercial SBA-15 > SBA-15 (8 g, 30 min) > SBA-15 (8 g, 90 min) > SBA-15 (8 g, 60 min). The order of the specific pore volumes from largest to smallest is Commercial SBA-15 > SBA-15 (8 g, 30 min) > SBA-15 (8 g, 60 min) > SBA-15 (8 g, 90 min). The order of pore wall thickness from thick to thin is Commercial SBA-15 > SBA-15 (8 g, 60 min) > SBA-15 (8 g, 90 min) > SBA-15 (8 g, 30 min). Among the synthesized SBA-15, the S_{BET} trends follow the crystallinity trend, which peaked in the SBA-15 (8 g, 30 min) sample. The crystallinity trend, on the other hand, does not appear to be linked to the D_{BJH}, V_{BJH}, and W_T trend.

The pore size distributions of SBA-15 synthesized with varying of sonication time and those of commercial SBA-15 are given in Fig. 10. The pore size distribution of SBA-15 (8 g, 30 min) (Fig. 10(a)) is similar to the pore size distribution of commercial SBA-15 (Fig. 10(d)), both having peaked at a pore diameter of about 5 nm. However, Fig. 10(d) is sharper with a higher peak intensity, which indicates that the uniformity of commercial SBA-15 is still higher than that of SBA-15 (8 g, 30 min). On the other hand, the pore size distributions of SBA-15 (8 g, 60 min) (Fig. 10(c)) and SBA-15 (8 g, 90 min) (Fig. 10(d)) are relatively wide, having peaked at 4.5 and 4 nm, respectively, with diameters ranging from 3 to 7 nm. Among the three synthesized materials, SBA-15 (8 g, 30 min) material has the highest pore volume at the same pore diameter, as demonstrated by the height

Table 4. The porosity of SBA-15 (8 g, 30 min), SBA-15 (8 g, 60 min), and SBA-15 (8 g, 90 min), and Commercial SBA-15

Sample	S_{BET} (m^2/g)	D_{BJH} (nm)	V_{BJH} (mL/g)	d_{100} (nm)	a_0 (nm)	W_T (nm)
SBA-15 (8 g, 30 min)	601	4.76	0.88	8.47	9.78	5.02
SBA-15 (8 g, 60 min)	635	3.98	0.65	8.89	10.27	6.29
SBA-15 (8 g, 90 min)	652	4.32	0.61	8.62	9.95	5.63
Commercial SBA-15	660	6.21	0.98	10.63	12.28	6.07

SBET : specific surface area, BET
D_{BJH} : pore diameter, BJH adsorption
V_{BJH} : specific pore volume
d_{100} : interplanar spacing
a_o : lattice parameter, for hexagonal = $2d_{100}/\sqrt{3}$
W_T : silica wall thickness, for hexagonal $W_T = a_0 - D$

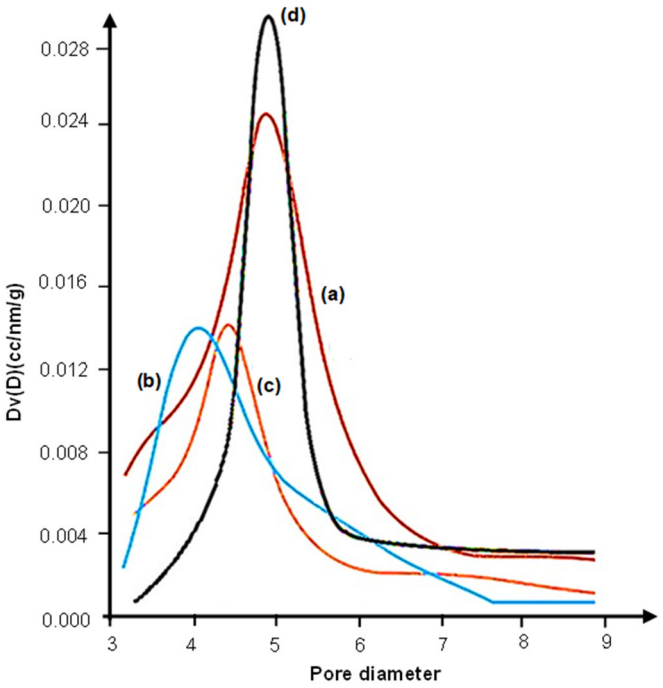

Fig 10. Pore size distribution of (a) SBA-15 (8 g, 30 min), (b) SBA-15 (8 g, 60 min), (c) SBA-15 (8 g, 90 min), and (d) Commercial SBA-15 samples

of its curve, which generally exceeds the other two curves. For the same pore diameter, SBA-15 (8 g, 30 min) has a longer pore length than SBA-15 (8 g, 60 min) and SBA-15 (8 g, 90 min).

Each sample of SBA-15 synthesized with this variation of sonication time has advantages in certain parameters, according to the porosity data in Table 4, but no sample is superior in all parameters. The most regular pore structure, as well as the largest pore diameter and specific pore volume, is found in sample SBA-15 (8 g, 30 min), however, it has the smallest specific surface area and thinnest pore wall. The pore structure of sample SBA-15 (8 g, 60 min) is fairly regular, with the thickest pore wall but the smallest pore diameter. The sample SBA-15 (8 g, 90 min) exhibited a higher specific surface area but a less uniform pore structure and the smallest specific pore volume. Overall, SBA-15 (8 g, 30 min) is the best of the three samples because it has the most regular pore structure, the largest pore diameter and specific pore volume, and takes the least amount of sonication time. Although not the best, the surface area and pore wall thickness of this sample were not substantially different from the others.

TEM analysis

The TEM image of SBA-15 (8 g, 30 min) and commercial SBA-15 (as a reference) are presented in Fig. 11. The TEM image of SBA-15 (8 g, 30 min) sample (Fig. 11(a)) reveals a significant degree of pore regularity although it is not as good as commercial SBA-15 (Fig. 11(b)). According to Fig. 11, the typical pore diameter and pore wall thickness of this material is around 5 and 5.5 nm, respectively. These results match well to those obtained by XRD and GSA data, indicating that the pore diameter and pore wall thickness of this material was 4.76 and 5.02 nm, respectively. For commercial SBA-15, TEM images show the pore diameter and wall thickness of 6.5 and 5 nm, respectively. This is also close to the results obtained from XRD and GSA data, which are 6.21 and 6.07 nm, respectively.

Table 5 compares the porosity of SBA-15 (8 g, 30 min) produced in this study to those achieved by other researchers employing a hydrothermal technique and a variety of silica sources [17-19,35-37], and also to the commercial SBA-15. The SBA-15 prepared in this work, i.e. SBA-15 (8 g, 30 min) which requires a shorter synthesis time and a less expensive silica source, is shown to be comparable to both those previously published in a

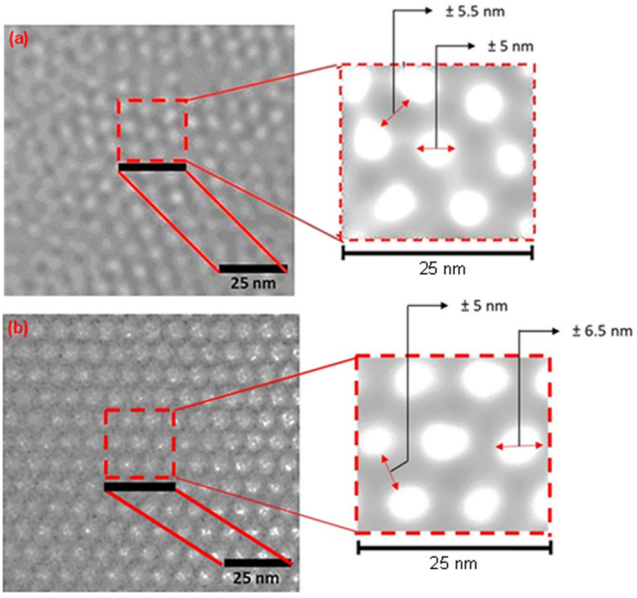

Fig 11. The TEM image of (a) SBA-15 (8 g, 30 min) and (b) commercial SBA-15

Table 5. the porosity of SBA-15 produced in the present research along with those obtained by other workers and the commercial SBA-15

Synthesis time (min)	Method	Silica source	S_{BET} (m^2 g^{-1})	D_{BJH} (nm)	V_{BJH} (cm^3/g)	Reference
1200	hydrothermal	TEOS	700	7	0.98	68
180	hydrothermal	TEOS	795	7.89	1.289	69
1440	hydrothermal	TEOS	948	5.5	1.3	70
4320	hydrothermal	TEOS	835	6.7	0.7	71
2880	hydrothermal	Rice husk silica	310	6.85	0.43	72
1440	hydrothermal	TEOS	558	6.5	0.8	73
1440	hydrothermal	Rice husk silica	656	11.73	1.092	74
1440	hydrothermal	Sodium silicate solution	869	5.7	1.24	75
1440	hydrothermal	TEOS	674	3.92	0.66	76
1440	hydrothermal	TEOS	1000	4.99	1.250	77
*	hydrothermal	TEOS	660	6.21	0.98	Commercial SBA-15
30	Sonochemical	Rice husk silica	601	4.76	0.88	This study

* There is no information

Table 6. the porosity of SBA-15 produced in the present research along with those obtained from many studies using the sonochemical method and TEOS as silica source, and the commercial SBA-15

Synthesis time (min)	Method	Silica source	S_{BET} (m^2 g^{-1})	D_{BJH} (nm)	V_{BJH} (cm^3/g)	Reference
60	Sonochemical	TEOS	562	4.7	0.65	78
120	Sonochemical	TEOS	606	4.9	0.74	78
180	Sonochemical	TEOS	618	4.6	0.72	78
240	Sonochemical	TEOS	570	4.4	0.62	78
60	Sonochemical	TEOS	760	6.5	0.76	42
*	Hydrothermal	TEOS	660	6.21	0.98	Commercial SBA-15
30	Sonochemical	Rice husk silica	601	4.76	0.88	This study

* There is no information

variety of publications as well as commercial SBA-15. As shown in Table 6, the porosity of SBA-15 (8 g, 30 min) obtained in this work is also comparable to the results of several works that use sonochemical method and TEOS as a silica source. Our results are generally comparable to those previously reported by some researchers [38-43], although we use non-commercial silica, extracted from rice husk. The successful use of low-cost materials such as rice husk silica with shorter synthesis times is promising and challenging for the future commercial synthesis of low-cost SBA-15.

■ CONCLUSION

SBA-15 has been successfully synthesized from rice husk silica utilizing a sonochemical method. The optimization of mass ratio of rice husk silica to surfactant (Pluronic P-123) and the sonication time has led to the more efficient and eco-friendly synthesis method. It has been observed that the amount of rice husk silica used and the sonication time have a significant impact on crystallinity, S_{BET}, D_{BJH}, V_{BJH}, W_T, and pore size distribution of the SBA-15 products. In general, the best results has been obtained from using 8 g of rice husk silica and a 30 min sonication time. The product has a specific surface area of 601 m^2 g^{-1}, a wall thickness of 5.02 nm, an average pore diameter of 4.76 nm, a specific pore volume of 0.88 mL g^{-1}, and a narrow pore size distribution (3–6.5 nm). The characteristics of the synthesized SBA-15 in this study are quite comparable to those of SBA-15 synthesized by using

commercial silica materials (TEOS) and the hydrothermal method, which consumes much more time and energy. In addition, the characteristics of SBA-15 synthesized in this study are also quite comparable to those of commercial SBA-15. Therefore, the synthesis method developed in this study is recommended to be used for further synthesis of SBA-15 because it is more efficient and environmentally friendly. The obtained SBA-15 from this study is potentially applied in the catalysis processes as well as in the adsorption study of hazardous pollutants such as heavy metals and dyes.

■ ACKNOWLEDGMENTS

The first author thanks and acknowledges financial support from the Universitas Gadjah Mada (UGM) Faculty of Mathematics and Natural Sciences through a BPPTNBH research grant with the contract number 87/J01.1.28/PL.06.02/2020. Thanks also to Wahyu Nugroho, A.Md., S.Si., and Kristiana Fajariatri, A.Md., S.Si., who have helped with this research.

■ REFERENCES

[1] Sun, L.B., Liu, X.Q., and Zhou, H.C., 2015, Design and fabrication of mesoporous heterogeneous basic catalysts, *Chem. Soc. Rev.*, 44 (15), 5092–5147.

[2] Sabbaghi, A., Lam, F.L.Y., and Hu, X.J., 2015, High Zr-loaded SBA-15 cobalt catalyst for efficient NO*x* reduction in lean-burn exhaust, *Appl. Catal., A*, 508, 25–36.

[3] Lai, Y.T., Chen, T.C., Lan, Y.K., Chen, B.S., You, J.H., Yang, C.M., Lai, N.C., Wu, J.H., and Chen, C.S., 2014, Pt/SBA-15 as a highly efficient catalyst for catalytic toluene oxidation, *ACS Catal.*, 4 (11), 3824–3836.

[4] Jiang, W.J., Yin, Y., Liu, X.Q., Yin, X.Q., Shi, Y.Q., and Sun, L.B., 2013, Fabrication of supported cuprous sites at low temperatures: an efficient, controllable strategy using vapor-induced reduction, *J. Am. Chem. Soc.*, 135 (22), 8137–8140.

[5] Buonomenna, M.G., Golemme, G., Tone, C.M., De Santo, M.P., Ciuchi, F., and Perrotta, E., 2013, Amine-functionalized SBA-15 in poly(styrene-*b*-butadiene-*b*-styrene) (SBS) yields permeable and selective nanostructured membranes for gas separation, *J. Mater. Chem. A*, 1 (38), 11853–11866.

[6] Yin, Y., Tan, P., Liu, X.Q., Zhu, J., and Sun, L.B., 2014, Constructing a confined space in silica nanopores: an ideal platform for the formation and dispersion of cuprous sites, *J. Mater. Chem. A*, 2 (10), 3399–3406.

[7] Yin, Y., Zhu, J., Liu, X.Q., Tan, P., Xue, D.M., Xing, Z.M., and Sun, L.B., 2016, Simultaneous fabrication of bifunctional Cu(I)/Ce(IV) sites in silica nanopores using a guests-redox strategy, *RSC Adv.*, 6 (74), 70446–70451.

[8] Vavsari, V.F., Ziarani, G.M., and Badiei, A., 2015, The role of SBA-15 in drug delivery, *RSC Adv.*, 5 (111), 91686–91707.

[9] Karnopp, J.C.F., Cardoso, T.F.M., Gonçalves, D., Carollo, A.R.H., de Castro, G.R., Duarte, A.P., and Martines, M.A.U., 2020, Preparation of the Rutin-SBA-16 drug delivery system, *J. Biomater. Nanobiotechnol.*, 11 (1), 1–13.

[10] Wang, J., Yang, M., Lu, Y., Jin, Z., Tan, L., Gao, H., Fan, S., Dong, W., and Wang, G., 2016, Surface functionalization engineering driven crystallization behavior of polyethylene glycol confined in mesoporous silica for shape-stabilized phase change materials, *Nano Energy*, 19, 78–87.

[11] Angioni, S., Villa, D.C., Cattaneo, A.S., Mustarelli, P., and Quartarone, E., 2015, Influence of variously functionalized SBA-15 fillers on conductivity and electrochemical properties of PBI composite membranes for high temperature polymer fuel cells, *J. Power Sources*, 294, 347–353.

[12] Pizzoccaro-Zilamy, M.A., Huiskes, C., Keim, E.G., Sluijter, S.N., van Veen, H., Nijmeijer, A., Winnubst, L., and Luiten-Olieman, M.W.J., 2019, New generation of mesoporous silica membranes prepared by a Stöber-solution pore-growth approach, *ACS Appl. Mater. Interfaces*, 11 (20), 18528–18539.

[13] Yang, J., Lin, G.S., Mou, C.Y., and Tung, K.L., 2020, Mesoporous silica thin membrane with tunable pore size for ultrahigh permeation and precise

molecular separation, *ACS Appl. Mater. Interfaces*, 12 (6), 7459–7465.

[14] Taweekarn, T., Wongniramaikul, W., Limsakul, W., Sriprom, W., Phawachalotorn, C., and Choodum, A., 2020, A novel colorimetric sensor based on modified mesoporous silica nanoparticles for rapid on-site detection of nitrite, *Microchim. Acta*, 187 (12), 643.

[15] Hassan, H.M., Ab Rahman, N.B., and Jalil, M.N., 2016, Mesoporous silica electrochemical sensors for the detection of ascorbic acid and uric acid, *Malays. J. Anal. Sci.*, 20 (2), 351–357.

[16] Linares, N., Silvestre-Albero, A.M., Serrano, E., Silvestre-Albero, J., and García-Martínez, J., 2014, Mesoporous materials for clean energy technologies, *Chem. Soc. Rev.*, 43 (22), 7681–7717.

[17] da Silva, F.C.M., Costa, M.J.S., da Silva, L.K.R., Batista, A.M., and da Luz, G.E., 2019, Functionalization methods of SBA-15 mesoporous molecular sieve: A brief overview, *SN Appl. Sci.*, 1 (6), 654.

[18] Selvakannan, P.R., Mantri, K., Tardio, J., and Bhargava, S.K., 2013, High surface area Au–SBA-15 and Au–MCM-41 materials synthesis: Tryptophan amino acid mediated confinement of gold nanostructures within the mesoporous silica pore walls, *J. Colloid Interface Sci.*, 394, 475–484.

[19] Costa, J.A.S., de Jesus, R.A., Santos, D.O., Mano, J.F., Romão, L.P.C., and Paranhos, C.M., 2020, Recent progresses in the adsorption of organic, inorganic, and gas compounds by MCM-41-based mesoporous materials, *Microporous Mesoporous Mater.*, 291, 109698.

[20] Gobara, H.M., 2016, Synthesis, mechanisms and different applications of mesoporous materials based on silica and alumina, *Egypt. J. Chem.*, 59 (2), 163–194.

[21] Zhang, H., Tang, C., Lv, Y., Sun, C., Gao, F., Dong, L., and Chen, Y., 2012, Synthesis, characterization, and catalytic performance of copper-containing SBA-15 in the phenol hydroxylation, *J. Colloid Interface Sci.*, 380 (1), 16–24.

[22] dos Santos, S.M.L., Nogueira, K.A.B., de Souza Gama, M., Lima, J.D.F., da Silva Júnior, I.J., and de Azevedo, D.C.S., 2013, Synthesis and characterization of ordered mesoporous silica (SBA-15 and SBA-16) for adsorption of biomolecules, *Microporous Mesoporous Mater.*, 180, 284–292.

[23] Schwanke, A.J., Favero, C., Balzer, R., Bernardo-Gusmão, K., and Pergher, S.B.C., 2018, SBA-15 as a support for nickel-based catalysts for polymerization reactions, *J. Braz. Chem. Soc.*, 29 (2), 328–333.

[24] Adrover, M.E., Pedernera, M., Bonne, M., Lebeau, B., Bucalá, V., and Gallo, L., 2020, Synthesis and characterization of mesoporous SBA-15 and SBA-16 as carriers to improve albendazole dissolution rate, *Saudi Pharm. J.*, 28 (1), 15–24.

[25] Thahir, R., Wahab, A.W., La Nafie, N., and Raya, I., 2019, Synthesis of high surface area mesoporous silica SBA-15 by adjusting hydrothermal treatment time and the amount of polyvinyl alcohol, *Open Chem.*, 17 (1), 963–971.

[26] Juárez-Serrano, N., Berenguer, D., Martínez-Castellanos, I., Blasco, I., Beltrán, M., and Marcilla, A., 2021, Effect of reaction time and hydrothermal treatment time on the textural properties of SBA-15 synthesized using sodium silicate as a silica source and its efficiency for reducing tobacco smoke toxicity, *Catalysts*, 11 (7), 808.

[27] Lázaro, A.L., Rodríguez-Valadez, F.J., López, J.J.M., and Espejel-Ayala, F., 2020, SBA-15 synthesis from sodium silicate prepared with sand and sodium hydroxide, *Mater. Res. Express*, 7, 045503.

[28] Norsurayaa, S., Fazlenaa, H., and Norhasyimia, R., 2016, Sugarcane bagasse as a renewable source of silica to synthesize Santa Barbara Amorphous-15 (SBA-15), *Procedia Eng.*, 148, 839–846.

[29] Nguyen, Q.N.K., Yen, N.T., Hau, N.D., and Tran, H.L., 2020, Synthesis and characterization of mesoporous silica SBA-15 and ZnO/SBA-15 photocatalytic materials from the ash of brickyards, *J. Chem.*, 2020, 8456194.

[30] Wang, J., Fang, L., Cheng, F., Duan, X., and Chen, R., 2013, Hydrothermal synthesis of SBA-15 using sodium silicate derived from coal gangue, *J. Nanomater.*, 2013, 352157.

[31] Razak, H., Abdullah, N., Setiabudi, H.N., Yee, C.S., and Ainirazali, N., 2019, Refluxed synthesis of SBA-15 using sodium silicate extracted from oil palm ash for dry reforming of methane, *Mater. Today: Proc.*, 19, 1363–1372.

[32] Rodrigues, J.J., Fernandes, F.A.N., and Rodrigues, M.G.F., 2018, Co/Ru/SBA-15 catalysts synthesized with rice husk ashes as silica source applied in the Fischer-Tropsch synthesis, *Braz. J. Pet. Gas*, 12 (3), 169–179.

[33] Liou, T.H., Tseng, Y.K., Liu, S.M., Lin, Y.T., Wang, S.Y., and Liu, R.T., 2021, Green synthesis of mesoporous graphene oxide/silica nanocomposites from rice husk ash: Characterization and adsorption performance, *Environ. Technol. Innovation*, 22, 101424.

[34] Watthanachai, C., Ngamcharussrivichai, C., and Pengprecha, S., 2018, Synthesis and characterization of bimodal mesoporous silica derived from rice husk ash, *Eng. J.*, 23 (1), 25–34.

[35] Fernandes, L.J., Calheiro, D., Sánchez, F.A.L., Camacho, A.L.D., de Campos Rocha, T.L.A., Moraes, C.A.M., and de Sousa, V.C., 2017, Characterization of silica produced from rice husk ash: Comparison of purification and processing methods, *Mater. Res.*, 20 (Suppl. 2), 512–518.

[36] Hossain, S.K.S., Mathur, L., and Roy, P.K., 2018, Rice husk/rice husk ash as an alternative source of silica in ceramics: A review, *J. Asian Ceram. Soc.*, 6 (4), 299–313.

[37] Xu, K., Sun, Q., Guo, Y., and Dong, S., 2013, Effects on modifiers on the hydrophobicity of SiO_2 films from nano-husk ash, *Appl. Surf. Sci.*, 276, 796–801.

[38] Laborte, A.G., Velasco, M.L., Wang, H., Behura, D., Pagnchak, M.R., Singh, H.N., Wardana, I.P., Vilayvong, S., and Shah, H., 2017, Release and adoption of improved cultivars in South and Southeast Asia: Rice, *The 9th ASAE International Conference: Transformation in Agricultural and Food Economy in Asia*, Bangkok, Thailand, 11-13 January 2017, 1455–1469.

[39] Barrera, D., Villarroel-Rocha, J., Marenco, L., Oliva, M.I., and Sapag, K., 2011, Non-hydrothermal synthesis of cylindrical mesoporous materials: Influence of the surfactant/silica molar ratio, *Adsorpt. Sci. Technol.*, 29 (10), 975–988.

[40] Yang, Q.Y., Zhu, H., Tian, L., Xie, S.H., Pei, Y., Li, H., Li, H.X., Qiao, M.H., and Fan, K.N., 2009, Preparation and characterization of Au-In/APTMS-SBA-15 catalysts for chemoselective hydrogenation of crotonaldehyde to crotyl alcohol, *Appl. Catal., A*, 369 (1-2), 67–76.

[41] Mollakarimi Dastjerdi, N., and Ghanbari, M., 2020, Ultrasound-promoted green approach for the synthesis of multisubstituted pyridines using stable and reusable SBA-15@ADMPT/$H_5PW_{10}V_2O_{40}$ nanocatalyst at room temperature, *Green Chem. Lett. Rev.*, 13 (3), 192–205.

[42] Prabhu, A., Sudha, V., Pachamuthu, M.P., Sundaravel, B., and Bellucci, S., 2022, Ultrasonic synthesis of Al-SBA-15 nanoporous catalyst for *t*-butylation of ethylbenzene, *J. Nanomater.*, 2022, 2512223.

[43] Li, J.Z., and Bai, X.F., 2017, Ultrasonic synthesis of Pd/SBA-15 catalyst for Suzuki-Miyaura coupling, *Adv. Eng. Res.*, 136, 454–457.

[44] Sun, S., Wang, S., Wang, P., Wu, Q., and Fang, S., 2015, Ultrasound assisted morphological control of mesoporous silica with improved lysozyme adsorption, *Ultrason. Sonochem.*, 23, 21–25.

[45] Ramos, J.M., Wang, J.A., Flores, S.O., Chen, L., Arellano, U., Noreña, L.E., González, J., and Navarrete, J., 2021, Ultrasound-assisted hydrothermal synthesis of V_2O_5/Zr-SBA-15 catalysts for production of ultralow sulfur fuel, *Catalysts*, 11 (4), 408.

[46] Yusof, N.S.M., Babgi, B., Alghamdi, Y., Aksu, M., Madhavan, J., and Ashokkumar, M., 2016, Physical and chemical effects of acoustic cavitation in selected ultrasonic cleaning applications, *Ultrason. Sonochem.*, 29, 568–576.

[47] Alshabanat, M., Al-Arrash, A., and Mekhamer, W., 2013, Polystyrene/montmorillonite nanocomposites: study of the morphology and effects of sonication time on thermal stability, *J. Nanomater.*, 2013, 650725.

[48] Shojaeiarani, J., Bajwa, D., and Holt, G., 2020, Sonication amplitude and processing time influence the cellulose nanocrystals morphology and dispersion, *Nanocomposites*, 6 (1), 41–46.

[49] Ali, F., Reinert, L., Lévêque, J.M., Duclaux, L., Muller, F., Saeed, S., and Shah, S.S., 2014, Effect of sonication conditions: solvent, time, temperature and reactor type on the preparation of micron sized vermiculite particles, *Ultrason. Sonochem.*, 21 (3), 1002–1009.

[50] Jokar, A., Azizi, M.H., Esfehani, Z.H., and Abbasi, S., 2017, Effects of ultrasound time on the properties of methylcellulose-montmorillonite films, *Int. Nano Lett.*, 7 (1), 59–68.

[51] Chaeronpanich, M., Nanta-ngern, A., and Limtrakul, J., 2007, Short-period synthesis of ordered mesoporous silica SBA-15 using ultrasonic technique, *Mater. Lett.*, 61 (29), 5153–5156.

[52] Banoth, S., Babu, V.S., Raghavendra, G., Rakesh, K., and Ojha, S., 2021, Sustainable thermochemical extraction of amorphous silica from biowaste, *Silicon*, 2021, s00240-021-01293-z.

[53] Yener, H.B., and Helvacı, Ş.Ş., 2015, Effect of synthesis temperature on the structural properties and photocatalytic activity of TiO_2/SiO_2 composites synthesized using rice husk ash as a SiO_2 source, *Sep. Purif. Technol.*, 140, 84–93.

[54] Ma, X., Zhou, B., Gao, W., Qu, Y., Wang, L., Wang, Z., and Zhu, Y., 2012, A recyclable method for production of pure silica from rice hull ash, *Powder Technol.*, 217, 497–501.

[55] Zemnukhova, L.A., Panasenko, A.E., Artem'yanov, A.P., and Tsoy, E.A., 2015, Dependence of porosity of amorphous silicon dioxide prepared from rice straw on plant variety, *BioResources*, 10 (2), 3713–3723.

[56] Palanivelu, R., Padmanaban, P., Sutha, S., and Rajendran, V., 2014, Inexpensive approach for production of high-surface-area silica nanoparticles from rice hulls biomass, *IET Nanobiotechnol.*, 8 (4), 290–294.

[57] Meléndez-Ortiz, H.I., Puente-Urbina, B., Castruita-de Leon, G., Mata-Padilla, J.M., and Garcia-Uriostegui, L., 2016, Synthesis of spherical SBA-15 mesoporous silica. Influence of reaction conditions on the structural order and stability, *Ceram. Int.*, 42 (6), 7564–7570.

[58] González, J., Wang, J.A., Chen, L., Manríquez, M., Salmones, J., Limas, R., and Arellano, U., 2018, Quantitative determination of oxygen defects, surface Lewis acidity, and catalytic properties of mesoporous MoO_3/SBA-15 catalysts, *J. Solid State Chem.*, 263, 100–114.

[59] Alavi, S., Hosseini-Monfared, H., and Siczek, M., 2013, A new manganese(III) complex anchored onto SBA-15 as efficient catalyst for selective oxidation of cycloalkanes and cyclohexene with hydrogen peroxide, *J. Mol. Catal. A: Chem.*, 377, 16–28.

[60] Hashemikia, S., Hemmatinejad, N., Ahmadi, E., and Montazer, M., 2015, Optimization of tetracycline hydrochloride adsorption on amino modified SBA-15 using response surface methodology, *J. Colloid Interface Sci.*, 443, 105–114.

[61] Gonzalez, G., Sagarzazu, A., Cordova, A. Gomes, M.E., Salas, J., Contreras, L., Noris-Suarez, K., and Lascano, L., 2018, Comparative study of two silica mesoporous materials (SBA-16 and SBA-15) modified with a hydroxyapatite layer for clindamycin controlled delivery, *Microporous Mesoporous Mater.*, 256, 251–265.

[62] Andrade, G.F., Gomide, V.S., da Silva Júnior, A.C., Goes, A.M., and de Sousa, E.M.B., 2014, An in situ synthesis of mesoporous SBA-16/hydroxyapatite for ciprofloxacin release: in vitro stability and cytocompatibility studies, *J. Mater. Sci.: Mater. Med.*, 25 (11), 2527–2540.

[63] Sheng, Y., Tang, X., Peng, E., and Xue, J., 2013, Graphene oxide based fluorescent nanocomposites for cellular imaging, *J. Mater. Chem. B*, 14 (4), 512–521.

[64] On, T.D., Zaidi, S.M.J., and Kaliaguine, S., 1998, Stability of mesoporous aluminosilicate MCM-41 under vapor treatment, acidic and basic conditions, *Microporous Mesoporous Mater.*, 22 (1-3), 211–224.

[65] Shirvanimoghaddam, K., Balaji, K.V., Yadav, R., Zabihi, O., Ahmadi, M., Adetunji, P., Naebe, M.,

2021, Balancing the toughness and strength in polypropylene composites, *Composites, Part B*, 223, 109121.

[66] Ramirez Mendoza, H., Jordens, J., Valdez Lancinha Pereira, M., Lutz, C., and Van Gerven, T., 2020, Effects of ultrasonic irradiation on crystallization kinetics, morphological and structural properties of zeolite FAU, *Ultrason. Sonochem.*, 64, 105010.

[67] Chagas, J.S., Almeida, J.N.S., Pereira, A.C.L., Medeiros, E.S., Silva Guedes de Lima, B.A., Ferreira e Santos, A.S., Oliveira, J.E., and Mattoso, L.H.C., 2019, Effect of sonication time interval on the size and crystallinity degree of cellulose nanocrystals, *Proceedings of the 18th Brazilian Material Research Society Meeting*, Rio de Janeiro, Brazil, 22-26 September 2019.

[68] Thielemann, J.P., Girgsdies, F., Schlögl, R., and Hess, C., 2011, Pore structure and surface area of silica SBA-15: Influence of washing and scale-up, *Beilstein J. Nanotechnol.*, 2, 110–118.

[69] Deryło-Marczewska, A., Zienkiewicz-Strzałka, M., Skrzypczyńska, K., Świątkowski, A., and Kuśmierek, K., 2016, Evaluation of the SBA-15 materials ability to accumulation of 4-chlorophenol on carbon paste electrode, *Adsorption*, 22 (4), 801–812.

[70] Mayani, S.V., Mayani, V.J., and Kim, S.W., 2014, SBA-15 supported Fe, Ni, Fe-Ni bimetallic catalysts for wet oxidation of bisphenol-A, *Bull. Korean Chem. Soc.*, 35 (12), 3535.

[71] Pérez-Vidal, H., Lunagómez, M.A., Pacheco, J.G., Torres-Torres, J.G., De la Cruz-Romero, D., Cuauhtémoc-López, I., and Beltramini, J.N., 2018, Co/SBA-15 modified with TMB in the degradation of phenol, *J. Appl. Res. Technol.*, 16 (5), 422–436.

[72] Lin, D., Huang, Y., Yang, Y., Long, X., Qin, W., Chen, H., Zhang, Q., Wu, Z., Li, S., Wu, D., Hu, L., Zhang, X., 2018, Preparation and characterization of highly ordered mercapto-modified bridged silsesquioxane for removing ammonia-nitrogen from water, *Polymers*, 10 (8), 819.

[73] Schwanke, A.J., Favero, C., Balzer, R., Bernardo-Gusmão, K., and Pergher, S.B.C., 2018, SBA-15 as a support for nickel-based catalysts for polymerization reactions, *J. Braz. Chem. Soc.*, 29 (2), 328–333.

[74] Liou, T.H., and Liou, Y.H., 2021, Utilization of rice husk ash in the preparation of graphene-oxide-based mesoporous nanocomposites with excellent adsorption performance, *Materials*, 14 (5), 1214.

[75] Mansour, S., Akkari, R., Chaabene, S.B., and Zina, M.S., 2020, Effect of surface site defects on photocatalytic properties of $BiVO_4/TiO_2$ heterojunction for enhanced methylene blue degradation, *Adv. Mater. Sci. Eng.*, 2020, 6505301.

[76] Kruatim, J., Jantasee, S., and Jongsomjit, B., 2016, Improvement of cobalt dispersion on Co/SBA-15 and Co/SBA-16 catalysts by ultrasound and vacuum treatments during post-impregnation step, *Eng. J.*, 21 (1), 17–28.

[77] Ruchomski, L., Pikula, T., Kamiński, D., Słowik, G., and Kosmulski, M., 2022, Synthesis and characterization of a novel composites derived from SBA-15 mesoporous silica and iron pentacarbonyl, *J. Colloid Interface Sci.*, 608, 2421–2429.

[78] Palani, A., Wu, H.Y., Ting, C.C., Vetrivel, S., Shanmugapriya, K., Chiang, A.S.T., and Kao, H.M., 2010, Rapid temperature-assisted sonochemical synthesis of mesoporous silica SBA-15, *Microporous Mesoporous Mater.*, 131 (1-3), 385–392.